PERGAMON

Chemical Engineering Science 57 (2002) 2169–2181

Chemical Engineering Science

www.elsevier.com/locate/ces

Dynamics analysis of an age distribution model of oscillating yeast cultures

Abdelqader M. Zamamiri[b], Yongchun Zhang[a], Michael A. Henson[c], Martin A. Hjortsø[a,*]

[a] *Department of Chemical Engineering, Louisiana State University, Baton Rouge, LA 70803, USA*
[b] *BioTechnology Institute, University of Minnesota, 1479 Gornter Ave. Ste. 240, Saint Paul, MN 55108, USA*
[c] *Department of Chemical Engineering, University of Massachusetts, Amherst, MA 01003-3110, USA*

Abstract

The ability of an age-population balance model to capture experimentally observed oscillatory dynamics of continuous cultures of budding yeast was investigated through numerical simulations. Experiments with continuous yeast cultures have shown that several oscillatory modes can occur at the same operating condition, and that the mode attained depends on the start-up conditions. Numerical simulations of the model did reveal the existence of several stable periodic solutions. However, each occurred over a different range of dilution rates. Experiments also have shown that the steady state in continuous yeast cultures is stable, even under conditions that allow oscillatory dynamics. The stability of the steady state of the age population balance model under conditions that allow oscillatory dynamics was not resolved. The Jacobian matrix at the steady state is highly ill conditioned, with some eigenvalues very close to the imaginary axis. Using different integration routines to solve the model gave different results with regard to the stability of the steady state, one solver finding the steady state to be stable, another finding the steady state to be unstable.

Keywords: Oscillating yeast culture; Age distribution; Bifurcation

1. Introduction

Baker's yeast *Saccharomyces cerevisiae* is an important microorganism in many industries including baking, food manufacturing, brewing and genetic engineering. Continuous cultures of *S. cerevisiae* can exhibit autonomous and sustained oscillations under glucose-limited aerobic conditions for a range of operating parameters (Alberghina, Ranzi, Porro, & Martegani, 1991; Chen, McDonald, & Bisson, 1990; Chen & McDonald, 1990; Martegani, Porro, Ranzi, & Alberghina, 1990; Münch, Sonnleitner, & Fiechter, 1991, 1992a, b; Parulekar, Semones, Rolf, Lievense, & Lim, 1986; Porro, Martegani, Ranzi, & Alberghina, 1988; Strässle, Sonnleitner, & Fiechter, 1988, 1989). Extracellular and intracellular parameters, such as the concentrations of evolved carbon dioxide, dissolved oxygen, glucose, ethanol, pH-controlling agent, storage carbohydrates, protein content, and cell mass as well as the budding index, exhibit oscillatory behavior. The oscillations are associated with a marked cell-cycle synchronization. These oscillations are referred to as cell-cycle dependent (Keulers, Satroutdinov, Suzuki, & Kuriyama, 1996) as opposed to other types of observed oscillations that do not result in cell-cycle synchrony (Keulers et al., 1996; Keulers, Suzuki, Satroutdinov, & Kuriyama, 1996; Goldbeter, 1996; Satroutdinov, Kuriyama, & Kobayashi, 1992). In most situations, control issues arise due to these oscillations as they adversely affect the stability and productivity of bioreactors (Martegani et al., 1990; Porro et al., 1988; Zhu, Zamamiri, Henson, & Hjortsø, 2000). In some situations, however, it might be desirable to induce and stabilize oscillations to increase the production of metabolites that are produced during a certain phase of the cell cycle (Zhu et al., 2000).

Many experimental studies have been conducted to investigate the cause of the autonomous oscillations and its stabilizing mechanisms (Alberghina et al., 1991; Chen et al., 1990; Chen & McDonald, 1990; Martegani et al., 1990; Münch et al., 1991, 1992a, b; Strässle et al., 1988, 1989; Keulers et al., 1996; Cazzador, Mariani, Martegani, & Alberghina, 1990). Based on these experiments, numerous conceptual and mathematical models were proposed to describe the oscillations (Martegani et al., 1990; Porro et al., 1988; Strässle et al., 1988, 1989; Cazzador et al., 1990; Hjortsø & Nielsen, 1994, 1995; Jones & Kompala, 1999; Kompala, 1999). The proposed models can be

* Corresponding author. Fax: +1-504-388-1476.
E-mail address: hjortso@che.lsu.edu (M. A. Hjortsø).

0009-2509/02/$ - see front matter
PII: S0009-2509(02)00109-4

generally classified into two categories: segregated models in which cell-cycle dynamics interact with medium components to cause the oscillations and stabilize the cell-cycle synchrony; and distributed, metabolic models in which bifurcation of metabolic kinetics cause the observed oscillations.

Recent experimental data from our lab (Zamamiri, Birol, & Hjortsø, 2001) indicate that different policies of chemostat start-up result in different final dynamical states. Two oscillatory states and a steady state were achieved at similar operating condition in three different experiments. These observations are not explained by models that oscillate through a Hopf bifurcation; in fact, there are no published distributed models known to us that can explain these observations. This leaves segregated mechanisms as possible explanations of these dynamics. The results presented in this paper do not allow one to draw conclusions about the right kind of model to be used, whether structured, distributed or segregated, because one cannot predict whether structured, distributed models will be discovered which are able to replicate the experimentally observed dynamics. Evidently, a "true" model will be a richly structured, segregated model in which the breakage and kinetic functions that appear in the population balance are modeled in terms of the cellular metabolism. Formulation of such models is a challenging task and, once formulated, obtaining their solutions in a reasonable time will be difficult with current computer power. It is, therefore, reasonable to ask, as is done in this paper, whether the simpler unstructured, segregated models can replicate the experimentally observed yeast dynamics.

In this work, an age distribution model is investigated for its ability to model the observed multiplicity of stable states. The aim of this study is not to obtain a quantitative fit of the model to the experimental data, but to determine whether the bifurcation dynamics of the age distribution model can reproduce the experimentally observed dynamics. A complete dynamics analysis of a population balance model is a very challenging task. The models have infinite dimensional state spaces so the basin of attraction of different attractors can be objects in infinite dimensional spaces and the models include kinetic functions that must be modeled or for which biologically reasonable expressions must be assumed. In this study, we investigate the existence of multiple stable states and explore the effect that changing the shape of the transition probabilities have on the dynamics and bifurcation behavior of the model. The model is based on population balance equations (PBE) coupled with a substrate balance. Since analytical solutions of population balance models for microbial growth can only be obtained under very restrictive simplifying assumptions (Hjortsø & Nielsen, 1994, 1995; Liou, Srienc, & Fredrickson, 1997), in this work a numerical solution of the model was obtained by the method of orthogonal collocation on finite elements (Rice & Do, 1995; Finlayson, 1980). The model predicts several oscillatory attractors, each of which is characterized by a unique structure of synchronized subpopulations of cells. Preliminary model simulations show that at some operating conditions, both a steady-state solution and a stable periodic solution exists, the attainment of either depends on the initial age distribution. However, the stability of the steady-state solution is questionable as will be discussed later. The simulations did not yield conditions that allowed the existence of two oscillatory states and one steady state as we have observed experimentally (Zamamiri et al., 2001).

The rest of the paper is organized in three sections. In Section 2, model development and the numerical solution method are reviewed. The results of model simulations and bifurcation analysis are discussed in Section 3. Finally, a summary is given in Section 4.

2. Model development and numerical solution method

2.1. Model development

Although a mathematical description of cell populations has been introduced more than three decades ago by Fredrickson, Ramkrishna, and Tsuchiya (1967), little application is found in biochemical engineering literature. There are two reasons that hindered the full utilization of population balances. First is the fact that the resulting partial integro-differential equations are difficult to solve. Second is the fact that application of the theory requires knowledge of three physiological functions that are difficult to determine experimentally (Srienc, 1999). These functions are the single-cell growth rate, the transition rates between different cell compartments, and the partitioning function which describes how a cell property (e.g. mass) of a dividing cell is partitioned among the two newborn cells (Srienc, 1999). In other particulate systems, the transition and partitioning functions are often called the breakage functions (Ramkrishna, 2000).

In the light of these facts, the use of age distribution models brings about several advantages that are worth mentioning. Unlike population balance models based on mass which give rise to partial integro-differential equations, models based on age are partial differential equations. This happens because all newborn cells have age zero and the integral term for the rate of formation of new cells appear as a boundary condition (the renewal equation) rather than in the population balance itself. Moreover, in age distribution models, two of the three physiological functions mentioned above need not be determined experimentally. First, the single-cell growth rate is simply unity and second, there are no partitioning functions since all cells are born at age zero. The transition functions, however, remains to be estimated. These functions are dependent on both the cell state (e.g. age or mass) and the environmental conditions. For modeling purposes, environmental conditions can be lumped in a single variable such as the substrate concentration. In the current modeling approach, no chemical structure is assumed for either the biophase or the

environment. Therefore, the model under study is a segregated unstructured model. This type of model is chosen because it is probably the simplest model form that is able to predict periodic behavior of the cell population and its relation to cell-cycle synchrony (Hjortsø & Nielsen, 1994, 1995).

The age distribution model is based on the following simplified cell cycle of budding yeast. The cycle is characterized by a critical cell mass m_c. Cells with mass greater than m_c are called mothers, while cells of lesser mass are called daughters. The point of the cell cycle when a cell reaches m_c is called the "Start" (Strässle et al., 1988; Hartwell & Unger, 1977; Lord & Wheals, 1980). Cells at the start grow for a period of time, U_p, before the emergence of a bud. Budded cells continue growing until the division age is reached. This period is referred to as budded phase period, B. At division, the bud separates forming a new daughter cell and the original mother cell is returned to the "Start" point of a new mother. In budding yeast, division is asymmetric as the newborn daughter cell is born at a smaller mass than the mother. Asymmetric division approaches symmetric division only at maximum growth rate (Hartwell & Unger, 1977; Lord & Wheals, 1980). Daughter cells grow until they reach m_c at which point they are considered as new mothers. Mother cells at the "Start" point have an age of zero. They grow until they reach the division age, at which point a mother cell divides into a daughter cell and a newborn mother cell, both at age zero. Daughter cells grow until they reach the transition age, the point at which they become mothers and their age is reset to zero.

This cell cycle is simplified in the sense that there is no distinction between budded and unbudded mother cells. This simplification should not impose a problem unless the environmental conditions become severely poor. Under poor conditions, unbudded mother cells rest in their current states and do not bud until the growth conditions improve. On the other hand, budded mother cells are committed to divide, and therefore, they grow for a specific period of time, divide and then rest at their newborn states.

The current model is an enhanced version of the age distribution model originally proposed by Hjortsø and Nielsen (1995). In the former model, both transition and division events occur at discrete ages (referred to as control points), while in the current model both events are modeled by probability functions. The enhancement make the model more biologically plausible since it accounts for individual differences between cells which cause the transition and division to occur over ranges of ages rather than at specific points. Another enhancement of the model is the incorporation of the substrate dependence of the transition probabilities by an effective substrate modeled as a second-order delay as opposed to a hard delay. The delay is needed to account for the fact that cell metabolism does not respond instantaneously to environmental changes. An effect similar to having a hard time delay can still be achieved by increasing the order of delay in the filtered signal.

Using the formulation of Fredrickson et al. (1967), the PBE for the age distributions of mothers and daughters, W_m and W_d, respectively, in a CSTR with dilution rate D are:

$$\frac{\partial W_m(a,t)}{\partial t} + \frac{\partial W_m(a,t)}{\partial a} = -[D + \Gamma_D(a, S^{(2)})]W_m(a,t), \tag{1}$$

$$\frac{\partial W_d(a,t)}{\partial t} + \frac{\partial W_d(a,t)}{\partial a} = -[D + \Gamma_T(a, S^{(2)})]W_d(a,t), \tag{2}$$

where a is the cell age and t is the time. The functions $\Gamma_D(a, S^{(2)})$ and $\Gamma_T(a, S^{(2)})$ are the division and transition intensity functions, respectively. The division intensity function is defined such that $\Gamma_D(a, S^{(2)})\,\mathrm{d}t$ is the probability that a mother cell with age a will divide in the next $\mathrm{d}t$ time interval. Similarly, $\Gamma_T(a, S^{(2)})\,\mathrm{d}t$ is the probability that a daughter cell with age a will become a mother in the next $\mathrm{d}t$ time interval. $S^{(2)}$ is the second-order filtered-substrate concentration, also referred to as the effective substrate concentration. To account for the influx of cells due to cell birth or cell transition, two more equations are needed. These equations are the renewal equations:

$$W_m(0,t) = W_{m0}(t) = \int_0^\infty \Gamma_D(a, S^{(2)})W_m(a,t)\,\mathrm{d}a + \int_0^\infty \Gamma_T(a, S^{(2)})W_d(a,t)\,\mathrm{d}a, \tag{3}$$

$$W_d(0,t) = W_{d0}(t) = \int_0^\infty \Gamma_D(a, S^{(2)})W_m(a,t)\,\mathrm{d}a. \tag{4}$$

The division and transition intensity functions are assumed to have the forms:

$$\Gamma_D(a, S^{(2)}) = \begin{cases} 0, & a \leqslant a_{cd}(S^{(2)}), \\ \alpha_d(a - a_{cd}(S^{(2)}))^{n_d}, & a_{cd}(S^{(2)}) < a \leqslant a_{cd}(S^{(2)}) + \delta_d, \\ \Gamma_{D_{\max}}, & a > a_{cd}(S^{(2)}) + \delta_d, \end{cases} \tag{5}$$

$$\Gamma_T(a, S^{(2)}) = \begin{cases} 0, & a \leqslant a_{ct}(S^{(2)}), \\ \alpha_t(a - a_{ct}(S^{(2)}))^{n_t}, & a_{ct}(S^{(2)}) < a \leqslant a_{ct}(S^{(2)}) + \delta_t, \\ \Gamma_{T_{\max}}, & a > a_{ct}(S^{(2)}) + \delta_t, \end{cases} \tag{6}$$

where $a_{cd}(S^{(2)})$ and $a_{ct}(S^{(2)})$ are the critical ages of division and transition, respectively, which are the ages beyond which cell division or cell transition commence. $\Gamma_{D_{\max}}$ and $\Gamma_{T_{\max}}$ are the maxima of the division and transition intensity functions, respectively. α_d, n_d, δ_d, α_t, n_t and δ_t are constant model parameters. δ_d and δ_t are chosen such that the intensity functions are piecewise continuous, giving rise to the expressions

$$\delta_d = \left(\frac{\Gamma_{D_{\max}}}{\alpha_d}\right)^{1/n_d} \quad \text{and} \quad \delta_t = \left(\frac{\Gamma_{T_{\max}}}{\alpha_t}\right)^{1/n_t}.$$

The critical ages of division and transition in this model were assumed to have analogous forms to the ages of division and transition functions in the original model (Hjortsø & Nielsen, 1995). However, the delayed substrate concentration was replaced by the effective substrate concentration as follows:

$$a_{cd}(S^{(2)}) = \pi_0 + \frac{\pi_1}{S^{(2)}}, \tag{7}$$

$$a_{ct}(S^{(2)}) = \frac{\pi_2}{S^{(2)}}. \tag{8}$$

These model equations were chosen because they are simple functional forms that reflect two important physiological phenomena. First, the division age typically increases when substrate concentration decreases, reflecting a lower population growth rate at lower substrate concentrations. Second, at the highest possible growth rates, which typically occur at high substrate concentrations, the transition age become so small that the division effectively becomes symmetric (Hartwell & Unger, 1977; Lord & Wheals, 1980). The delayed response is accounted for by the use of the effective substrate concentration instead of the actual concentration. π_0, π_1, and π_2 are constant model parameters.

The substrate balance equation is written as

$$\frac{dS}{dt} = D(S_f - S) - \frac{1}{\lambda_m(S)}\int_0^\infty W_m(a,t)\,da - \frac{1}{\lambda_d(S)}\int_0^\infty W_d(a,t)\,da, \tag{9}$$

where S is the actual substrate concentration, S_f the feed substrate concentration and $\lambda_m(S)$ and $\lambda_d(S)$ the yield coefficients for mothers and daughters, respectively. The integrals appearing in the second and third terms on the right-hand side of Eq. (9) are the zeroth moments of the mother's and daughter's cell age distributions, which by definition are the mother's and daughter's cell number concentrations, respectively. The yield coefficients are assumed to have the form

$$\lambda_m(S) = \frac{K_m + S}{\mu_m S}, \tag{10}$$

$$\lambda_d(S) = \frac{K_d + S}{\mu_d S}, \tag{11}$$

where K_m, μ_m, K_d and μ_d are constant parameters. The yield coefficients are the rate of increase in cell age divided by the rate of substrate consumption. The rate of increase in cell age is unity and the λ's are, therefore, the inverse of the rate of substrate consumption by cells of age a. Modeling the rate of substrate consumption by the commonly used Monod rate expression, Eqs. (10) and (11) were obtained.

The filtered substrate concentrations are written as

$$\frac{dS^{(1)}}{dt} = \alpha(S - S^{(1)}), \tag{12}$$

$$\frac{dS^{(2)}}{dt} = \alpha(S^{(1)} - S^{(2)}), \tag{13}$$

Table 1
Model parameters

Parameter	Value
K_d	20.0 g/l
K_m	20.0 g/l
α	2.5 h^{-1}
μ_d	4.7e-11 g/h
μ_m	4.7e-11 g/h
π_0	1.5 h
π_1	0.5 h g/l
π_0	3.0 h g/l

Table 2
Parameters of the transition and division intensity functions

Moderate intensity functions			
Γ_{T1}		Γ_{D1}	
n_T	4	n_D	4
α_T	300 h^{-5}	α_D	300 h^{-5}
$\Gamma_{T\max}$	20 h^{-1}	$\Gamma_{D\max}$	20 h^{-1}
δ_T	0.51 h	δ_D	0.51 h
Sharp intensity functions			
Γ_{T2}		Γ_{D2}	
n_T	3	n_D	3
α_T	800 h^{-4}	α_D	800 h^{-4}
$\Gamma_{T\max}$	20 h^{-1}	$\Gamma_{D\max}$	20 h^{-1}
δ_T	0.29 h	δ_D	0.29 h

where $S^{(1)}$ is the first-order filtered-substrate concentration and α the adaptivity constant which determine how rapidly cells respond to environmental changes (Stephens & Lyberatos, 1987).

The values of the model parameters are given in Table 1. Two sets of transition and division intensity functions were used in model simulations and system analysis. These sets of intensity functions differ only in the values of their parameters as shown in Table 2. The intensity functions are referred to as moderate and sharp depending on the size of the age interval over which the function increase from 0 to its maximum. The parameter values were not obtained by a fit to the experimental data but were found by trial and error to produce biologically reasonable results.

2.2. Numerical solution

The current model consists of a coupled set of nonlinear algebraic, ordinary differential, and partial differential equations. An analytical solution of the model is not possible, and therefore, numerical solution is needed to perform model simulations and bifurcation analysis. Possible candidate numerical methods are the method of finite differences (MFD) and the method of weighted residuals (MWR) (Rice & Do, 1995; Finlayson, 1980). In general, pure finite differences schemes do not result in satisfactory solutions for PBE

models due to various reasons, such as numerical instabilities, low accuracy, and lack of dissipativity, which call for the use of special "hybrid" MFD (Mantzaris, Liou, Daoutidis, & Srienc, 1999). The use of the method of weighted residuals for solving mass PBE models was illustrated by Subramanian and Ramkrishna (1971). The method of orthogonal collocation is a variation of MWR. In this method, the model is approximated by coupled, ordinary differential equations (ODEs) for the values of the dependent variable at the collocation points. The method is easy to apply and program for this problem and the solution at any point can be obtained from the values of the dependent variables at the collocation points. The method of orthogonal collocation is also superior to finite differences in terms of stability because it uses the information from all collocation points, instead of just neighboring points, to estimate the derivatives at each point (Rice & Do, 1995). In this work, the method of orthogonal collocation on finite elements was employed to obtain the numerical solution desired. In orthogonal collocation on finite elements, the domain of the problem is divided into subdomains (called elements) and the method of orthogonal collocation is applied on each subdomain. This variation is particularly useful for problems with sharp variations in the distribution of states (Rice & Do, 1995) such as our problem.

The method of orthogonal collocation on finite elements was found to provide stable and robust solutions of the age distribution model. The method divides the mother's and daughter's age domains into elements and further discretizes the elements into a number of internal collocation points and two boundary points. From this point onwards, we will refer to all the internal collocation points and the boundary points simply as collocation points, unless otherwise specified. The partial derivative of W_m or W_d with respect to age at a collocation point in a specific element is approximated by a linear combination of the age distribution values at all the collocation points in that element, except for the lower boundary of the first element in each domain. The elements are constructed such that the lower boundary of the first element starts at age zero, and therefore, at these two boundaries the renewal equations are applied. Consequently, the method approximates the PBEs by coupled sets of ODEs for the values of the distribution of states at the collocation points. Integral terms are approximated by the Gaussian quadrature (Finlayson, 1980). The resulting nonlinear ODEs in vector–matrix notation have the form

$$\frac{\mathrm{d}}{\mathrm{d}t}\mathbf{W}_m = -\mathbf{A}_m\mathbf{W}_m - D\mathbf{W}_m - \mathbf{\Gamma}_D\mathbf{W}_m - W_{m0}\mathbf{A}_{m0}, \tag{14}$$

$$\frac{\mathrm{d}}{\mathrm{d}t}\mathbf{W}_d = -\mathbf{A}_d\mathbf{W}_d - D\mathbf{W}_d - \mathbf{\Gamma}_T\mathbf{W}_d - W_{d0}\mathbf{A}_{d0}, \tag{15}$$

where $\mathbf{W}_m$ and $\mathbf{W}_d$ are the column vectors of the mother's and daughter's age distribution values at each collocation point, starting from the second collocation point in each domain. The first collocation points in the mother's and daughter's domains are $a_{m0} = 0$ and $a_{d0} = 0$, respectively. $\mathbf{A}_m$ and $\mathbf{A}_d$ are the first derivative weight matrices in the mother's and daughter's domains, respectively. $\mathbf{\Gamma}_D$ and $\mathbf{\Gamma}_T$ are the diagonal matrices of the division and transition intensity functions. $\mathbf{\Gamma}_D$ is defined such that the element $\mathbf{\Gamma}_{D(i,\,i)}$ is $\Gamma_D(a_{mi}, S^{(2)})$. $\mathbf{\Gamma}_T$ is defined in a similar manner in the daughter's domain. W_{m0} and W_{d0} are the mother's and daughter's age distribution values at a_{m0} and a_{d0}, respectively. $\mathbf{A}_{m0}$ is a column vector that accounts for the contribution of W_{m0} to the derivatives in the first finite element in the mother's domain and $\mathbf{A}_{d0}$ accounts for the corresponding contribution of W_{d0} in the first element in the daughter's domain.

The renewal equations are written as

$$W_{m0}(t) = \sum_{i=1}^{N_m} wg_m(a_{mi})\Gamma_D(a_{mi}, S^{(2)})W_m(a_{mi}, t) + \sum_{i=1}^{N_d} wg_d(a_{di})\Gamma_T(a_{di}, S^{(2)})W_d(a_{di}, t), \tag{16}$$

$$W_{d0}(t) = \sum_{i=1}^{N_m} wg_m(a_{mi})\Gamma_D(a_{mi}, S^{(2)})W_m(a_{mi}, t), \tag{17}$$

where N_m and N_d are the total number of collocation points in the mother's and daughter's domains, respectively. a_{mi} and a_{di} are the ages at collocation point i in the mother's and daughter's domains, respectively. wg_m and wg_d are the vectors of quadrature weights in the mother's and daughter's domains, respectively. The substrate balance is written as

$$\frac{\mathrm{d}S}{\mathrm{d}t} = D(S_f - S) - \frac{1}{\lambda_m(S)}\sum_{i=0}^{N_m} wg_m(a_{mi})W_m(a_{mi}, t) - \frac{1}{\lambda_d(S)}\sum_{i=0}^{N_d} wg_d(a_{di})W_d(a_{di}, t). \tag{18}$$

The rest of the model equations are unchanged.

2.2.1. Model simulations

Model simulations were performed using MATLAB. The model equations were solved using ODE15s, a stiff ODE solver. An analytical expression of the Jacobian matrix was supplied to the solver. In the previous work, we have used a mesh of fixed equal-sized elements to solve a mass PBE model of budding yeast using the method of orthogonal collocation on finite elements (Zhu et al., 2000). In the current study, dynamic meshes of 15 elements in the mother's domain and 18 elements in the daughter's domain were used. Each element had 3 internal collocation points obtained as the roots of the appropriate Jacobi polynomials (Rice & Do, 1995). The total number of collocation points in the mother's domain is $N_m = 61$ and in the daughter's domain is $N_d = 73$. The state vector of the resulting ODE model consists of the cell age distribution at each collocation point as well as the substrate concentration and the first- and second-order

filtered-substrate concentrations. In the placement of the elements, each domain is divided into three subdomains. The first, subdomain 1, extends from $a = 0$ to $(a = a_c - 0.2)$ or $(a = a_c - 0.3)$ h, where a_c is the critical age of either transition or division. Subdomain 2 starts at the end of subdomain 1 and extends for 1.4 h. Finally, subdomain 3 starts at the end of subdomain 2 and extends for 1 h. The distribution of states changes most rapidly in subdomain 2 as the intensity functions sharply increase from zero to their maxima. Therefore, at least one-third of the elements are stacked in subdomain 2. All the transition and division events are expected to take place in subdomain 2. However, one finite element is placed in subdomain 3 to take care of any remaining cells as an extra precaution. The rest of the elements are placed in subdomain 1. If the element size in subdomain 1 is smaller than that in subdomain 2, some elements are transferred to subdomain 2, where they are needed most. The positioning of the elements is not fixed. The critical ages are checked every one virtual hour in each domain. If in either domain, the current value of the critical age deviates more than 0.1 h from its value 1 h in the past, the position of the elements in that domain will be altered accordingly. Performing this check more frequently than once every virtual hour resulted in much longer execution times with no clear benefits. The values at the new collocation points are obtained using Lagrange interpolating polynomials in each element (Chapra & Canale, 1998). If the new age domain is larger than the old one, the age distribution is set to zero at the new age collocation points that exceed the range of the old domain.

2.2.2. Bifurcation analysis

The bifurcation analysis was done using code provided by Professor Yannis Kevrekidis, (Princeton). The shooting method was used to perform the continuation steps in the bifurcation analysis. The continuation code was written in FORTRAN and it uses the stiff ODE solver ODESSA with explicit simultaneous sensitivity analysis to solve the ODE model. An analytical expression of the Jacobian matrix was also supplied to the ODE solver. For every oscillatory attractor, the code requires a guess of the initial age distribution and the period, which were obtained from MATLAB simulation results. The same number of elements and internal collocation points as used in model simulations are used here. For the bifurcation analysis, however, simpler fixed meshes were utilized. The end of each age domain was fixed and the elements were distributed such that the last hour of each domain was a single element, and the remaining elements were equally divided in the rest of the domain.

3. Results and discussion

3.1. Simulation results

Oscillatory solutions occur less readily in the current model than in the simplified control point model (Hjortsø & Nielsen, 1995) due to the dispersive effect of the transition and division intensity functions. In the current study, two sets of intensity functions were investigated, the parameters of which are given in Table 2. The sharpness of the functions are related to the rate at which the function increases from zero to its maximum value. Since the maximum values for all the intensity functions used were chosen to be the same, the sharpness of these functions are directly related to the parameters δ_T and δ_D. The smaller the values of δ_T and δ_D, the sharper are the transition and division intensity functions. Stable oscillatory solutions were still possible even in the case of moderate transition and division intensity functions Γ_{T1} and Γ_{D1}. However, further increase in δ_T and δ_D led to the loss of periodic solutions.

Using the moderate intensity functions Γ_{T1} and Γ_{D1}, two periodic attractors were found at the feed substrate concentration $S_f = 30$ g/l. By a periodic or oscillatory attractor we mean the set of oscillatory solutions which are characterized by a specific subpopulations structure in the mother's and daughter's domains. The N:M attractor is the set of oscillatory solutions with N subpopulations in the mother's domain, as indicated by N local maxima in the mother's age distribution, and M subpopulations in the daughter's domain (Hjortsø & Nielsen, 1994, 1995). Fig. 1 depicts the age distributions of 1:2 and 1:3 attractors. The periodic attractors were found in two separate regions of dilution rate (D) values. Typical oscillation patterns in the substrate concentration (S) and cell number concentrations (N_c) for the 1:2 attractor at $D = 0.15\ \mathrm{h}^{-1}$ are shown in Fig. 1. The figure also shows the corresponding oscillations at $D = 0.095\ \mathrm{h}^{-1}$, which belong to the 1:3 attractor. Naturally, the mother's and daughter's age distributions associated with the oscillatory patterns shown in Fig. 1 are time varying. However, a representative snapshot of the age distributions in each case is shown below their respective patterns.

The continuation code utilizing the shooting method was employed to determine the whole range of limit cycles in a given attractor. The code requires an initial age distribution and a reasonably "good" guess of the period, which were readily available from MATLAB simulations. The results obtained from the continuation code were in good agreement with those obtained from MATLAB simulations. The maximum and minimum values of the periodic solutions of S and N_c obtained from MATLAB simulations at discrete values of D are shown as (•) in Fig. 2 for the 1:2 and 1:3 attractors. The dashed lines in Fig. 2 represent the results obtained from the continuation code and the solid line represents the steady-state profile. At steady state, the equations of the PBE model become a set of nonlinear algebraic equations coupled with two ODEs. With the type of expressions used in this analysis, an analytical solution for the steady-state profile, which is shown in Fig. 2, was possible. It was found that all the system variables oscillate around their steady-state values.

When the simulations were performed using the sharp intensity functions Γ_{T2} and Γ_{D2}, the regions of D

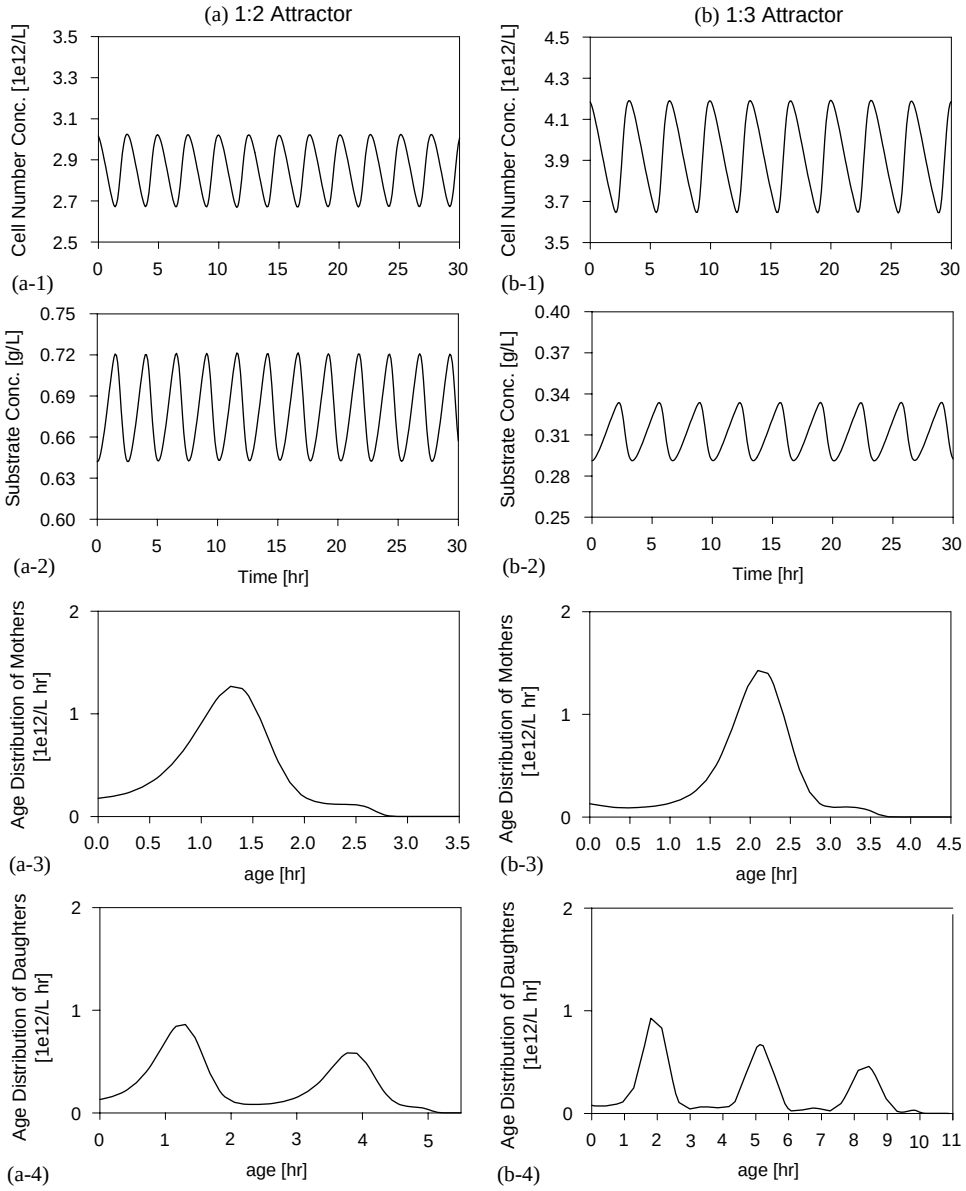

Fig. 1. Typical oscillation patterns associated with the 1:2 attractor (a) and 1:3 attractor (b). At $S_f = 30$ g/l, and $D = 0.15\ \mathrm{h}^{-1}$ a periodic solution that belongs to the 1:2 attractor is obtained. Oscillations are observed in all system parameters such as cell number concentration (a-1) and substrate concentration (a-2). The 1:2 attractor is characterized by one subpopulation of mothers (a-3) and two subpopulations of daughters (a-4). At $D = 0.095\ \mathrm{h}^{-1}$, a periodic solution that belongs to the 1:3 attractor is obtained. Oscillations are also observed in all system parameters such as cell number concentration (b-1) and substrate concentration (b-2). The 1:3 attractor is characterized by one subpopulation of mothers (b-3) and three subpopulations of daughters (b-4).

supporting the 1:2 and 1:3 attractors expanded and shifted towards higher values of D. The ranges of D supporting the 1:2 attractor under the moderate and sharp intensity function conditions are compared in Fig. 3. In addition to the original two attractors a third 1:1 attractor was found. The bifurcation diagram representing the 1:1 and 1:2 attractors is shown in Fig. 4. The discovery of the 1:1 attractor is not surprising. It has the simplest structure of the three attractors, and intuitively it was expected to be the easiest attractor to locate. However, all our attempts to locate the 1:1 attractor using the moderate Γ_{T1} and Γ_{D1} failed. In fact, the 1:1 attractor may not exist when this moderate division intensity is used. The locus of the 1:1 attractor was found at higher dilution rates than the other attractors, and at higher values of dilution rate, the average substrate and effective substrate concentrations are also higher. This results in smaller averages for the critical ages of division and transition, a_{cd} and a_{ct}, than at lower values of the dilution rate. The range of ages over which the mother and daughter distribution functions, W_m and W_d, are significantly different from zero is directly related to a_{cd} and a_{ct}, and both ranges are smaller at higher dilution rates than at lower dilution rates. Consequently, the intensity functions become relatively more dispersive at higher dilution rates,

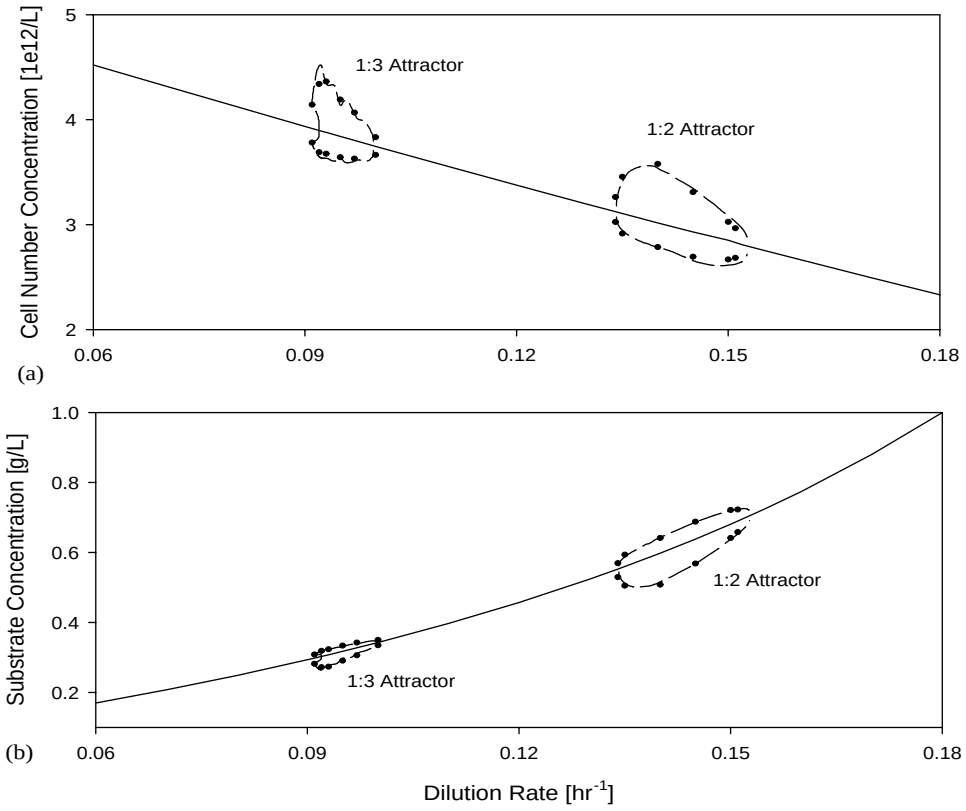

Fig. 2. Bifurcation diagram at $S_f = 30$ g/l obtained by employing moderate intensity functions Γ_{T1} and Γ_{D1}. Bifurcations are shown in terms of cell number concentration (a) and substrate concentration (b). The diagram shows maximum and minimum cell number and substrate concentration during the oscillations obtained from MATLAB (•), maximum and minimum cell number and substrate concentrations during the oscillations obtained from the continuation code (- -) and the steady-state profiles (—).

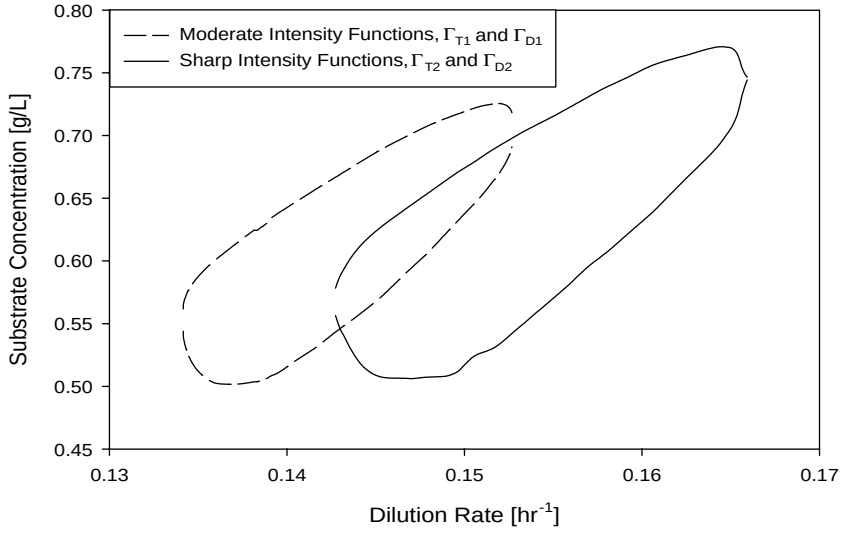

Fig. 3. The effect of the "sharpness" of intensity functions on the range of dilution rates supporting the 1:2 attractor. The curves show the maximum and minimum values of the substrate concentration during the oscillations under moderate intensity functions (Γ_{T1} and Γ_{D1}) (- -) and sharp intensity functions (Γ_{T2} and Γ_{D2}) (—) parameter values.

eliminating stable oscillatory solutions. In other words, the size of δ_T and δ_D is only a relative measure of the sharpness of Γ_T and Γ_D, and hence the "sharpness" of Γ_T and Γ_D with fixed δ_T and δ_D is not the same in all attractors. The sharpness of the intensity functions should be thought of as the ratio of δ_T and δ_D to the age domains of W_d and W_m, respectively. Of course, this reasoning is only valid when the transition intensity functions, Eqs. (5) and (6), are not

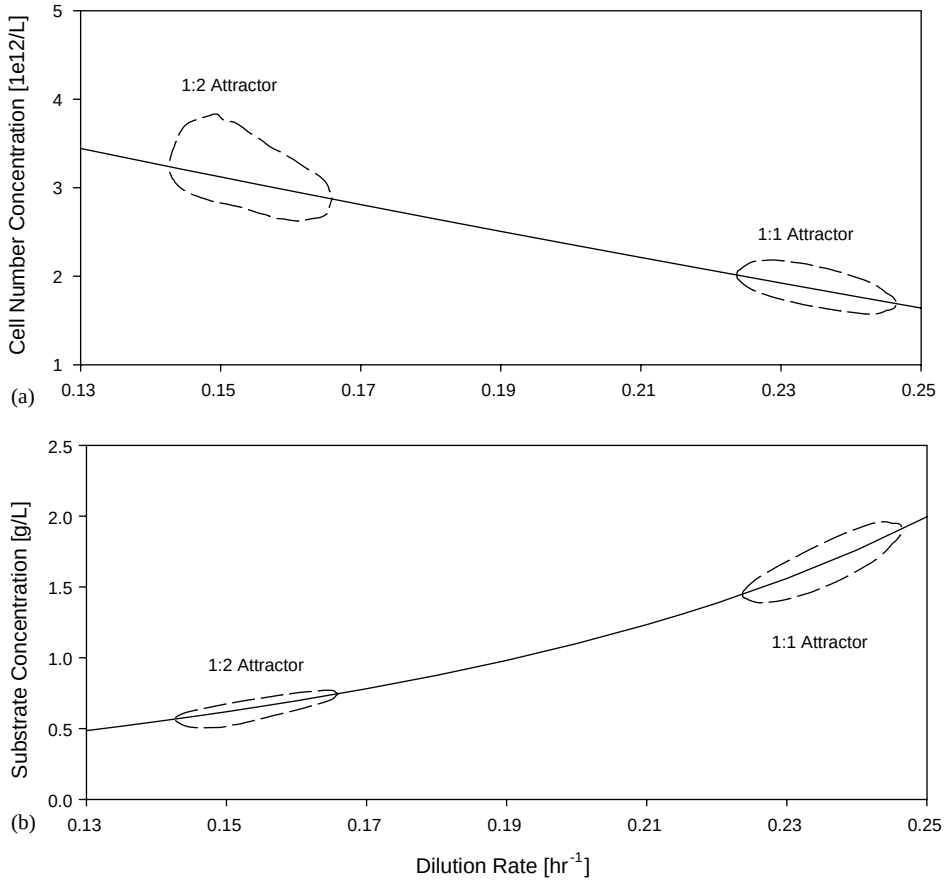

Fig. 4. Bifurcation diagram at $S_f = 30$ g/l, obtained by employing sharp intensity functions Γ_{T1} and Γ_{D1}. The diagram represents the 1:1 and 1:2 attractors in terms of cell number concentration (a) and substrate concentration (b). The diagram shows maximum and minimum cell number and substrate concentration during the oscillations obtained from the continuation code (- -) and the steady-state profiles (—).

functions of the dilution rate, substrate or effective substrate concentrations.

The effect of the feed substrate concentration (S_f) on the range of D supporting the oscillatory attractors was investigated. Three levels of S_f were studied: 15, 30 and 60 g/l. It was found that the ranges of D at which the attractors exist decrease with increasing S_f. As a matter of fact, we were unable to locate the 1:3 attractor at $S_f = 60$ g/l. Fig. 5 shows the effect of increasing S_f on the domain of the 1:2 attractor in terms of D. The upper bifurcation point of D is almost the same in all three cases. However, periodic dynamics start to appear at lower values of D at lower S_f. It should be noted that increasing S_f does not affect the steady-state value of S, and neither does it affect the average substrate concentration for an oscillating culture. Therefore, the decrease in the domain of the 1:2 attractor is not due to any change in the values of the critical ages or the relative sharpness of the intensity functions. The effect of increasing the feed substrate concentration is directly translated into an increase in the steady-state value of the cell number concentration, or the average cell number concentration for an oscillating culture. In this case, the reduction of the 1:2 attractor domain is attributed solely to the change in operating conditions.

The results obtained from model simulation indicate the existence of multiple oscillatory attractors, which has been confirmed experimentally. In our experiments, however, the different attractors have been observed at similar operating conditions, while in simulations the ranges of D supporting the different attractors do not intersect. However, it has been demonstrated that the domains of the oscillatory attractors are strong functions of both model parameters and operating conditions. Therefore, reproduction of experimental observations is conceivable given sufficient time and computing power to adjust the model parameters and transition probabilities.

3.2. Bifurcation analysis results

In our effort to investigate the bifurcation dynamics of continuous yeast cultures, an experiment was performed in which the periodic dynamics of an oscillating chemostat culture was quenched by slowly reducing the dilution rate to a value that did not support oscillations. The chemostat was run for 2 days at the new conditions, then the dilution rate was increased slowly (so as to keep the system at a quasi-steady state) to its original value. The non-oscillatory

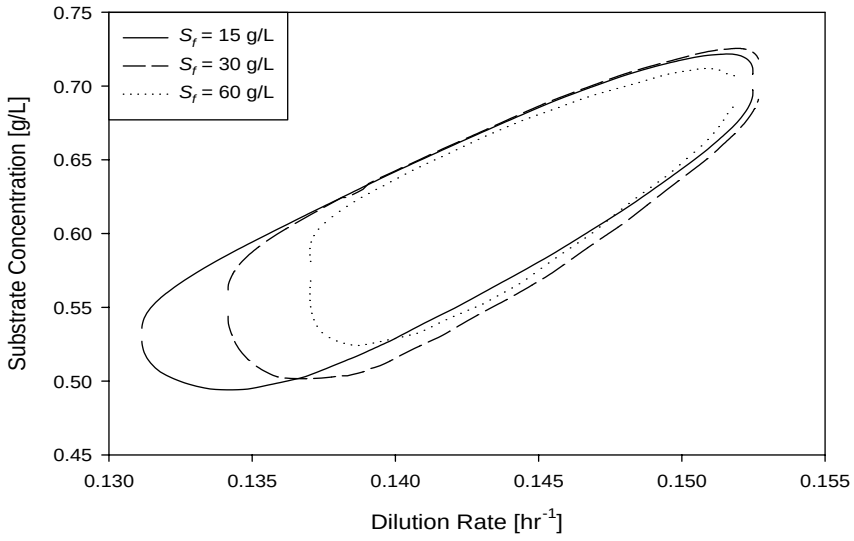

Fig. 5. The effect of feed substrate concentration, S_f, on the range of dilution rates supporting the 1:2 attractor. The curves show the maximum and minimum values of the substrate concentration during the oscillations at $S_f = 15$ g/l (—), 30 g/l (- -) and 60 g/ l (· · ·).

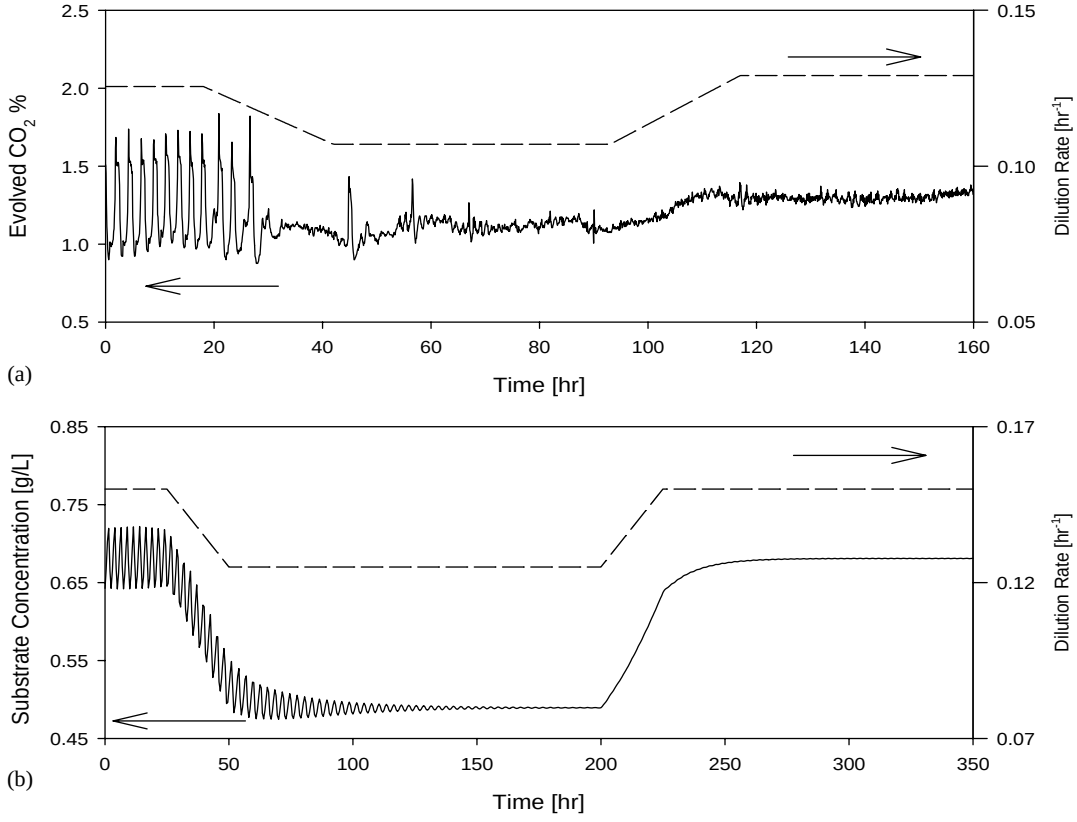

Fig. 6. Bifurcation dynamics of budding yeast investigated experimentally (a) indicate that an oscillatory state and a steady state can be achieved at the same operating conditions. Model simulations (b) predict the same bifurcation mechanisms. In the top figure, the actual response of CO_2 concentration in the exit gas stream (—) to set point changes in the dilution rate (- -) is shown. In the bottom figure, the corresponding simulated response of substrate concentration (—) to changes in dilutions rate (- -) is shown.

state was preserved throughout the ramp, and it was sustained at the original dilution rate for almost three more days. A simulation of the experiment was performed and the results obtained were qualitatively similar to those obtained experimentally. Both experimental data for the CO_2 in the outlet gas stream and the corresponding model simulations in terms of substrate concentration are shown in Fig. 6.

From nonlinear system dynamics viewpoint, since the model predicts the existence of a stable limit cycle that

encircles a stable steady state, one expects an unstable limit cycle somewhere between the two stable solutions (Khalil, 1996). A powerful feature of the continuation code is its ability to find both stable and unstable limit cycles. At the end points of the dilution rate region within which oscillatory attractors exist, the stable limit cycle shrinks and approaches the steady state. If an unstable limit cycle exists between the stable limit cycle and the stable steady state, the continuation code is expected to find it near those points. In all the attractors studied, attempts of finding such unstable limit cycles were unsuccessful. However, when the amplitude of the oscillations diminish as the limit cycles approach the steady state, it becomes increasingly tedious and time consuming to perform the analysis. At these points, smaller step sizes should be specified among other adjustments to the code parameters. The stable limit cycle keeps getting smaller until it collapses to the steady state. The failure of the continuation code in finding the unstable limit cycles brings us back to examine the original assumption that the steady state is indeed stable.

Model simulations with MATLAB show that the system remains at steady state for hundreds of virtual hours when the initial condition is the analytical steady-state distribution. Further simulations indicated that the system still arrives to the steady-state solution even if small disturbances were introduced to the initial steady-state distribution. These simulations indicate the stability of the steady state, and the existence of at least a small region of attraction for this state. However, the eigenvalues of the Jacobian matrix tell another story. When the eigenvalues of the Jacobian matrix were evaluated at $S_f = 30$ g/l, $D = 0.14\ \mathrm{h}^{-1}$ and the corresponding steady-state distribution, a pair of the eigenvalues was found in the right half-plane. The pair was very close to the imaginary axis and the value of the real part, 0.0090, was very small compared to the real part of smallest negative eigenvalue, -55.0729. The condition number of the Jacobian matrix also was very large, 1.565×10^{27}, indicating that the Jacobian matrix was ill conditioned. To investigate whether the discretizing process has an effect on the position of the pair of eigenvalues with positive real part, we have further discretized the system using 22 elements in the mothers' domain and 25 elements in the daughters' domain with 3 internal collocation points in each element. One pair of positive eigenvalues was found with a very small real part of 0.0095 compared to the real part of the smallest eigenvalue of -75.2900. Once again, the Jacobian matrix was found to be ill conditioned. Considering the small magnitude of the positive eigenvalues, the ill condition of the Jacobian matrices and the error involved in determining their eigenvalues, one can only have limited confidence in the Jacobian matrix analysis. The pair of positive eigenvalues might actually lie on the imaginary axis, in which case the stability of the system cannot be inferred from the Jacobian matrix but requires analysis of the higher order terms of the Taylor expansions of the ODEs.

Finally, the ODE integrator used in the continuation code, ODESSA, was used to integrate the model equations starting with the steady-state distribution as the initial condition. Again, the system remained at steady state for hundreds of virtual hours. However, there was a significant difference between the solutions obtained using the MATLAB ODE solver, ODE15s, and the ODESSA solver. By magnifying the observed steady-state signals for substrate concentration, MATLAB simulations reveal a small converging oscillatory signal, while simulations using ODESSA reveal a small diverging oscillatory signal as shown in Fig. 7. The solutions obtained using the ODESSA solver, therefore, indicate that the steady state is not stable. The observations above, although not conclusive, raise reasonable doubt about the stability of the steady state.

Assuming that the unstable limit cycle, indeed, does not exist as the results of the continuation code imply, the steady state must then become unstable as the oscillations emerge. In most of the attractors studied, the stable limit cycles branch from the steady state and collapse back at the steady state which is a characteristic of the supercritical Hopf bifurcation (Looss & Joseph, 1980). Only the 1:3 attractor at $S_f = 30$ g/l and the 1:2 attractor at $S_f = 60$ g/l obtained under moderate intensity functions parameters show the Hopf bifurcations that are subcritical at one end and supercritical at the other end (Looss & Joseph, 1980). Even at the end that shows a subcritical Hopf bifurcation, the stable limit cycle becomes very small before it branches to an unstable limit cycle that persists for a very small range of the bifurcation parameter before it collapses back at the steady state. In all cases, however, the bifurcation mechanism observed was a Hopf bifurcation.

Our results raise three questions: (i) is the steady state predicted by the model stable or not? (ii) is the steady state observed experimentally stable or not? and (iii) is it justified to eliminate models just on the basis of their bifurcation mechanisms? More specifically, is it justified to eliminate all models that bifurcate through a Hopf bifurcation mechanism? The answer to the first question is that we do not know. Different numerical methods give different and conflicting answers about the stability of the steady state. However, the important common fact revealed by both methods is that the system has very slow dynamics and whether the steady state is stable or not, very little change is observed in the steady-state conditions even for extended periods of time. This does raise the possibility that the experimentally observed steady states are in fact not stable, but are bifurcating extremely slowly to an oscillatory state. However, this conclusion is contrary to the previous observations that oscillations appear or disappear very rapidly based on environmental conditions (Münch et al., 1992a). In the previous work (Birol, Zamamiri, & Hjortsø, 2000), we have observed that the actual system is also characterized by long transients. For instance, FFT analysis revealed that the transients in the oscillatory state take almost 2 days to die out. Therefore, the currently observed non-oscillatory state which

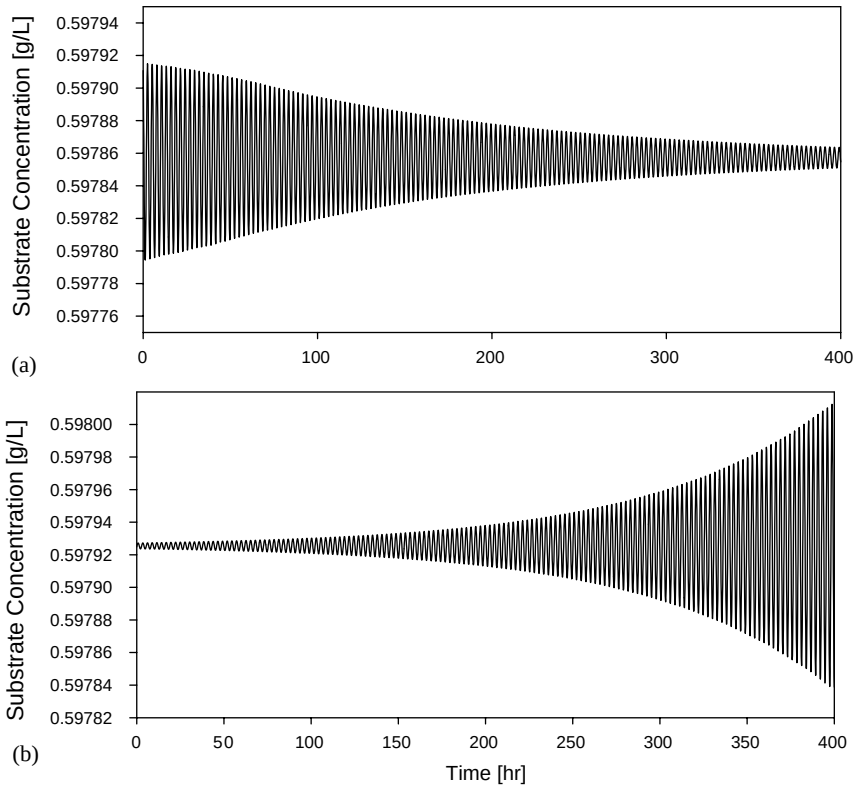

Fig. 7. Results of model simulations performed at $S_f = 30$ g/l and $D = 0.14\ \mathrm{h}^{-1}$ and starting with the corresponding steady-state distribution as the initial condition. Model equations were integrated using MATLAB stiff ODE solver, ODE15s (a) and the continuation code ODE solver, ODESSA (b). The simulations show that the steady state can be observed for hundreds of virtual hours (note the range on the substrate concentration axis); however, simulations performed using ODE15s predict a stable steady state, while simulations performed using ODESSA predict an unstable steady state.

persisted for several days may be a true stable steady state or just an extended transient. More experimental work is required to investigate the stability of this state. Finally, the bifurcation mechanism underlying the emergence of oscillations in a certain model does not reveal the whole picture. Knowing that a model bifurcates through a Hopf bifurcation, for example, does not reveal how many oscillatory solutions are possible, or how rapidly the steady state bifurcates to the oscillatory state. Therefore, more information about model bifurcation than just its bifurcation mechanism may be needed in order to validate or discard the model. Performing a detailed bifurcation analysis is a very useful tool in model discrimination. However, care should be taken not to generalize the conclusions about the validity of a specific model based solely on its bifurcation mechanism.

4. Summary

An age distribution PBE model was proposed as an explanation of the autonomous oscillations in budding yeast. The model was solved numerically by the method of orthogonal collocation on finite elements. The model predicts the existence of multiple oscillatory attractors, an observation that is experimentally validated. However, in the model simulations the attractors occur at different dilution rates while experimentally observed oscillatory modes have been observed at the same dilution rate. The range of dilution rates supporting the attractors depend on values of model parameters, the proposed mathematical expressions of different biological functions and the operating conditions. The model also predicts the existence of a stable oscillatory state and a prolonged steady state at the same operating conditions in good agreement with experimental observations. There is conflicting evidence about the stability of the steady state, however. The system dynamics are very slow and the apparent steady state can persist for extended periods of time. A detailed bifurcation analysis can be a useful tool for model discrimination, although care should be taken in drawing conclusions about the validity of models based solely on their bifurcation mechanism.

Acknowledgements

Financial support from National Science Foundation, Grants BES-9522274 and CTS-9501368, is gratefully acknowledged. We thank Prof. Ioannis Kevrekidis and Krishnan Sankaranarayanan (Princeton) for providing the continuation code and for their assistance with the calculations using this code.

References

Alberghina, L., Ranzi, B. M., Porro, D., & Martegani, E. (1991). Flow cytometry and cell cycle kinetics in continuous and fed-batch fermentations of budding yeast. *Biotechnological Progress*, *7*, 299–304.

Birol, G., Zamamiri, A. M., & Hjortsø, M. A. (2000). Frequency analysis of autonomously oscillating yeast cultures. *Process Biochemistry*, *35*, 1085–1091.

Cazzador, L., Mariani, L., Martegani, E., & Alberghina, L. (1990). Structured segregated models and analysis of self-oscillating yeast continuous cultures. *Bioprocess Engineering*, *5*, 175–180.

Chapra, S., & Canale, R. (1998). *Numerical methods for engineers*. New York: McGraw-Hill.

Chen, C.-I., & McDonald, K. A. (1990). Oscillatory behavior of *Saccharomyces cerevisiae* in continuous culture: II. Analysis of cell synchronization and metabolism. *Biotechnology and Bioengineering*, *36*, 28–38.

Chen, C.-I., McDonald, K. A., & Bisson, L. (1990). Oscillatory behavior of *Saccharomyces cerevisiae* in continuous culture: I. Effects of pH and nitrogen levels. *Biotechnology and Bioengineering*, *36*, 19–27.

Finlayson, B. A. (1980). *Nonlinear analysis in chemical engineering*. New York: McGraw-Hill.

Fredrickson, A. G., Ramkrishna, D., & Tsuchiya, H. M. (1967). Statistics and dynamics of procaryotic cell populations. *Mathematical Biosciences*, *1*, 327–374.

Goldbeter, A. (1996). *Biochemical oscillations and cellular rhythms*. Cambridge, UK: Cambridge University Press.

Hartwell, L. H., & Unger, M. W. (1977). Unequal division in *Saccharomyces cerevisiae* and its implications for the control of cell division. *Journal of Cell Biology*, *75*, 422–435.

Hjortsø, M. A., & Nielsen, J. (1994). A conceptual model of autonomous oscillations in microbial cultures. *Chemical Engineering Science*, *49*, 1083–1095.

Hjortsø, M. A., & Nielsen, J. (1995). Population balance models of autonomous microbial oscillations. *Journal of Biotechnology*, *42*, 255–269.

Jones, K. D., & Kompala, D. S. (1999). Cybernetic model of the growth dynamics of *Saccharomyces cerevisiae* in batch and continuous cultures. *Journal of Biotechnology*, *71*, 105–131.

Keulers, M., Satroutdinov, A. D., Suzuki, T., & Kuriyama, H. (1996). Synchronization affector of autonomous short-period-sustained oscillation of *Saccharomyces cerevisiae*. *Yeast*, *12*, 673–682.

Keulers, M., Suzuki, T., Satroutdinov, A. D., & Kuriyama, H. (1996). Autonomous metabolic oscillations in continuous culture of *Saccharomyces cerevisiae* grown on ethanol. *FEMS Microbiology Letters*, *142*, 253–258.

Khalil, H. (1996). *Nonlinear systems*. Upper Saddle River, NJ: Prentice-Hall.

Kompala, D. S. (1999). Cybernetic modeling of spontaneous oscillations in continuous cultures of *Saccharomyces cerevisiae*. *Journal of Biotechnology*, *71*, 267–274.

Liou, J. J., Srienc, F., & Fredrickson, A. G. (1997). Solution of population balance models based on a successive generation approach. *Chemical Engineering Science*, *52*, 1529–1540.

Looss, G., & Joseph, D. D. (1980). *Elementary stability of bifurcation theory*. New York: Springer.

Lord, P. G., & Wheals, A. E. (1980). Asymmetric division of *Saccharomyces cerevisiae*. *Journal of Bacteriology*, *142*, 808–818.

Mantzaris, N. V., Liou, J.-J., Daoutidis, P., & Srienc, F. (1999). Numerical solution of a mass structured cell population balance model in an environment of changing substrate concentration. *Journal of Biotechnology*, *71*, 157–174.

Martegani, E., Porro, D., Ranzi, B. M., & Alberghina, L. (1990). Involvement of a cell size control mechanism in the induction and maintenance of oscillations in continuous cultures of budding yeast. *Biotechnology and Bioengineering*, *36*, 453–459.

Münch, T., Sonnleitner, B., & Fiechter, A. (1991). Cell cycle of synchronously cultivated *Saccharomyces cerevisiae*. In M. Reuss, H. Chmiel, E. Gilles, & H. Knackmuss (Eds.), *Biochemical Engineering Stuttgart* (pp. 373–376). New York: Gustav Fischer Stuttgart.

Münch, T., Sonnleitner, B., & Fiechter, A. (1992a). The decisive role of the *Saccharomyces cerevisiae* cell cycle behaviour for dynamic growth characterization. *Journal of Biotechnology*, *22*, 329–352.

Münch, T., Sonnleitner, B., & Fiechter, A. (1992b). New insights into the synchronization mechanism with forced synchronous cultures of *Saccharomyces cerevisiae*. *Journal of Biotechnology*, *24*, 299–314.

Parulekar, S. J., Semones, G. B., Rolf, M. J., Lievense, J. C., & Lim, H. C. (1986). Induction and elimination of oscillations in continuous cultures of *Saccharomyces cerevisiae*. *Biotechnology and Bioengineering*, *28*, 700–710.

Porro, D., Martegani, E., Ranzi, B. M., & Alberghina, L. (1988). Oscillations in continuous cultures of budding yeast: A segregated parameter analysis. *Biotechnology and Bioengineering*, *32*, 411–417.

Ramkrishna, D. (2000). *Population balances theory and applications to particulate systems in engineering*. San Diego, CA: Academic Press.

Rice, R. G., & Do, D. D. (1995). *Applied mathematics and modeling for chemical engineers*. New York: Wiley.

Satroutdinov, A. D., Kuriyama, H., & Kobayashi, H. (1992). Oscillatory metabolism of *Saccharomyces cerevisiae* in continuous culture. *FEMS Microbiology Letters*, *98*, 261–268.

Srienc, F. (1999). Cytometric data as the basis for rigorous models of cell population dynamics. *Journal of Biotechnology*, *71*, 233–238.

Stephens, M. L., & Lyberatos, G. (1987). Effect of cycling on final mixed culture fate. *Biotechnology and Bioengineering*, *29*, 672–678.

Strässle, C., Sonnleitner, B., & Fiechter, A. (1988). A predictive model for the spontaneous synchronization of *Saccharomyces cerevisiae* grown in continuous culture. I. Concept. *Journal of Biotechnology*, *7*, 299–318.

Strässle, C., Sonnleitner, B., & Fiechter, A. (1989). A predictive model for the spontaneous synchronization of *Saccharomyces cerevisiae* grown in continuous culture. II. Experimental verification. *Journal of Biotechnology*, *9*, 191–208.

Subramanian, G., & Ramkrishna, D. (1971). On the solution of statistical models of cell populations. *Mathematical Biosciences*, *10*, 1–23.

Zamamiri, A. Q., Birol, G., & Hjortsø, M. A. (2001). Multiple stable states and hysteresis in continuous. oscillating cultures of budding yeast. *Biotechnology and Bioengineering*, *75*, 305–312.

Zhu, G.-Y., Zamamiri, A. M., Henson, M. A., & Hjortsø, M. A. (2000). Model predictive control of continuous yeast bioreactors using cell population balance models. *Chemical Engineering Science*, *55*, 6155–6167.